Editors' Suggestion

Strong Coupling of a Single Ion to an Optical Cavity

Hiroki Takahashi,* Ezra Kassa, Costas Christoforou, and Matthias Keller
Department of Physics and Astronomy, University of Sussex, Brighton BN1 9QH, United Kingdom

(Received 15 April 2019; published 2 January 2020)

Strong coupling between an atom and an electromagnetic resonator is an important condition in cavity quantum electrodynamics. While strong coupling in various physical systems has been achieved so far, it remained elusive for single atomic ions. Here, we achieve a coupling strength of $2\pi \times (12.3 \pm 0.1)$ MHz between a single $^{40}Ca^{+}$ ion and an optical cavity, exceeding both atomic and cavity decay rates which are $2\pi \times 11.5$ and $2\pi \times (4.1 \pm 0.1)$ MHz, respectively. We use cavity assisted Raman spectroscopy to precisely characterize the ion-cavity coupling strength and observe a spectrum featuring the normal mode splitting in the cavity transmission due to the ion-cavity interaction. Our work paves the way towards new applications of cavity quantum electrodynamics utilizing single trapped ions in the strong coupling regime for quantum optics and quantum technologies.

DOI: 10.1103/PhysRevLett.124.013602

Coupling between atoms and electromagnetic fields is a ubiquitous physical process that underlies a plenitude of electromagnetic phenomena. In cavity quantum electrodynamics (CQED), this interaction is studied in its simplest form where a single atomic emitter is coupled to well-defined electromagnetic modes of a resonator [1,2]. In many applications of CQED, the coherent atom-photon interaction rate needs to exceed the decoherence rates of the system. This so-called strong coupling regime has been attained in many physical systems including neutral atoms [3,4], solid state systems [5–8], and an ensemble of trapped ions [9]. Strongly coupled light-matter systems resulted in remarkable applications such as a one-atom optical switch [10] and a quantum optical circulator [11]. However, despite decade-long attempts [9,12–20] strong coupling has remained elusive for single trapped ions until now.

Because of their outstanding properties such as long coherence times [21] and high-fidelity quantum controls [22], trapped ions are a leading system for optical atomic clocks [23,24], quantum metrology [25,26], and quantum computation [27,28]. The setting of CQED brings about exciting possibilities to connect individual quantum devices by providing efficient quantum interfaces with optical photons [29]. Compared to single ions in free space [30,31], the entanglement generation efficiency of remote ions based on strongly coupled ion-cavity systems is enhanced by orders of magnitude [32]. This enables the distributed architecture for large-scale quantum information processing using photonic networks [33]. Here, by coupling a single ion to an optical cavity in the strong coupling regime for the first time, we demonstrate a key milestone for this enabling technology.

In the past, Fabry-Perot cavities with macroscopic mirrors were successfully combined with ion traps [14,17,18]. In these experiments, however, the ion-cavity coupling was in the weak coupling regime. Since the emitter-cavity coupling scales as $\propto 1/\sqrt{V_m}$ where V_m is the cavity's mode volume, it is essential to reduce V_m to achieve strong coupling. The main challenge in ion-cavity systems is to achieve small mode volume without disturbing the trapping field when incorporating dielectric mirrors near the trapping region. Employing laser machined fiber-based Fabry-Perot cavities (FFPCs) has proven to be a viable solution for this purpose and resulted in several successful implementations recently [19,20,34]. However, none of these experiments achieved a coupling strength which exceeds the atomic and cavity decay rates simultaneously. Based on the ion trap with an integrated FFPC presented in [34] and the technique to precisely position the ion in the cavity field [35], in this work we achieve a coherent ion-cavity coupling of $g = 2\pi \times (12.3 \pm 0.1)$ MHz greater than both the atomic decay rate of the $P_{1/2}$ state of $\gamma = 2\pi \times 11.5$ MHz [36] and the cavity decay rate of $\kappa = 2\pi \times (4.1 \pm 0.1)$ MHz [32]. This gives us a cooperativity $(=g^2/\gamma\kappa)$ of 3.2, on a par with the highest value achieved for an ion-cavity system [17] but with a considerably higher photon extraction rate.

Our experimental apparatus is an endcap-style Paul trap for $^{40}Ca^{+}$ ions with an integrated FFPC [see Fig. 1(a) and [32,34,35] for more details]. The FFPC is coupled to the electronic transition between the $P_{1/2}$ and $D_{3/2}$ states at 866 nm [see Fig. 1(b)]. The cavity field decay rate κ is measured to be $2\pi \times (4.1 \pm 0.1)$ MHz [32]. Two radial electrodes (RE3 and RE4) are used to displace the rf potential minimum by applying signals synchronous and in phase to the main drive [35] (RE1 and RE2 are used for micromotion compensation). In this way the ion is translated radially without incurring excess micromotion. Using a trapped ion as a probe for the cavity field [35], we

 © 2020 American Physical Society

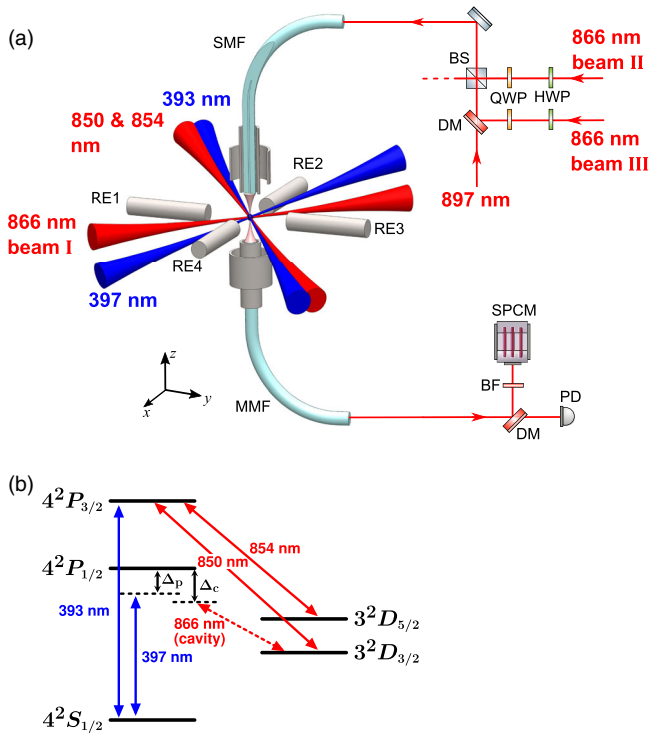

FIG. 1. (a) A schematic of the experimental setup. BF, bandpass filter; BS, beam splitter; DM, dichroic mirror; HWP, half-wave plate; MMF, multimode fiber; PD, photodiode; QWP, quarter-wave plate; RE, radial electrode; SMF, single-mode fiber; SPCM, single-photon counting module. (b) Energy levels of $^{40}Ca^+$ ion with driving lasers and the cavity on the relevant transitions.

determine that the center of the TEM_{00} cavity mode is located at $(3.4 \pm 0.1, 6.4 \pm 0.3)$ μm in the x and y directions, respectively, from the ion's original position when RE3 and RE4 are grounded. The ion is Doppler cooled on the $S_{1/2} - P_{3/2}$ transition with a laser at 393 nm to circumvent inefficient cooling on the $S_{1/2} - P_{1/2}$ transition caused by the strong Purcell effect when the cavity is near resonant on the $P_{1/2} - D_{3/2}$ transition [34]. Lasers at 850 and 854 nm repump the ion from the metastable D states into the $S_{1/2}$ state. Three laser beams at 866 nm (beams I, II, and III) with individual polarization controls are used for optical pumping and probing of the ion. Two of them (beams II and III) are injected into the input SM fiber to drive the FFPC. A laser beam at 897 nm is also sent into the FFPC through the SM fiber with its transmission used to stabilize the length of the FFPC.

Having moved the ion to the radial center of the FFPC, we now characterize g_0 with the optimized overlap at the antinode of the cavity. The ion-cavity coupling is quantified by analyzing the single-photon emission spectra of the ion-cavity system. Figure 2(a) shows the pulse sequences of the lasers for this measurement. In combination with the cavity locked close to the $P_{1/2} - D_{3/2}$ transition with a detuning Δ_c, a short pulse of the 397 nm laser with a detuning Δ_p results in a single photon in the cavity via a vacuum-stimulated Raman transition from the $S_{1/2}$ to the $D_{3/2}$ state [14]. Normally the Raman resonance condition dictates $\Delta_p = \Delta_c$. However, due to the dressing of the ion's states by the cavity photons, the resonance frequency of the $P_{1/2} - D_{3/2}$ transition and therefore the Raman resonance are shifted [37]. Figure 2(b) shows a spectrum of single-photon emission as a function of Δ_c while Δ_p is fixed at -10 MHz. It can be clearly seen that the peak frequency of the spectrum is shifted by an amount δ from the expected $\Delta_p = \Delta_c$ condition. We repeat this Raman spectroscopy for different Δ_p as shown in Fig. 2(c) to measure the dependence of δ on Δ_p. The frequency shift δ exhibits a dispersionlike profile whose amplitude and gradient depend on the magnitude of g_0. Because δ also depends on the Rabi frequency Ω_{397} of the 397 nm laser through its own ac Stark shift, we independently measure Ω_{397} to be $2\pi \times (11.9 \pm 0.4)$ MHz by the electron shelving method employed in [34]. Given Ω_{397} and other known experimental parameters such as the beam detunings, beam polarizations, and the magnetic field, the single-photon emission spectrum and hence δ can be precisely simulated by solving time-dependent master equations with g_0 as the only free parameter [see the inset of Fig. 2(d) and [32]]. Utilizing the dependence of δ on g_0 and fitting this numerical model to the experimental data as shown in Fig. 2(d), we obtain the coherent ion-cavity coupling $g_0 = 2\pi \times (15.1 \pm 0.1)$ MHz [32].

A small magnetic field (= 0.9 G) is applied to align the quantization axis to the cavity axis such that the cavity supports two distinct polarizations σ_+ and σ_-. As shown in Fig. 3(a), the ion is simultaneously coupled to these two polarization modes on the transitions connecting the Zeeman sublevels in the $P_{1/2}$ and $D_{3/2}$ state manifolds. This configuration effectively realizes a closed three-level lambda system interconnected via a bimodal cavity. When a two-level atom is coupled to a single optical mode, there are two dressed states $(|g,1\rangle + |e,0\rangle)/\sqrt{2}$ and $(|g,1\rangle - |e,0\rangle)/\sqrt{2}$ with an energy gap $2g$ ($\hbar = 1$) in the subspace for the first excitation from the ground state $(= |g,0\rangle)$ [see Fig. 3(b)]. Here, g and e denote the ground and excited states of the atom, respectively, and 0 and 1 denote the intracavity photon number. As a result, a coherent oscillation between $|g,1\rangle$ and $|e,0\rangle$ occurs at the vacuum Rabi frequency of $2g$. Similarly, for the bimodal system with three atomic levels, the subspace for the first excitation includes three originally degenerate states $|a,1,0\rangle$, $|b,0,1\rangle$, and $|c,0,0\rangle$. Here, the notation indicates a product of the atomic state and the photon number states of the two cavity modes [see Fig. 3(c)]. Because of the atom-cavity coupling, the system now has three dressed states $|u_+\rangle$, $|u_-\rangle$, and $|u_0\rangle$:

$$|u_\pm\rangle = \frac{g_1|a,1,0\rangle + g_2|b,0,1\rangle \pm \lambda|c,0,0\rangle}{\sqrt{2}\lambda}, \qquad (1)$$

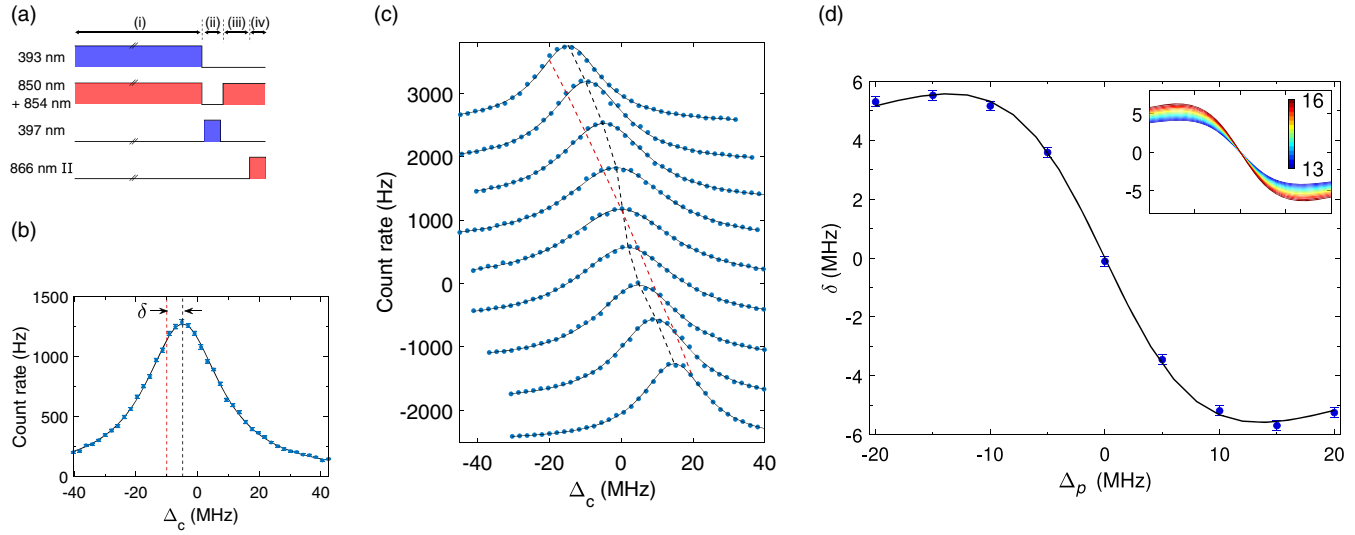

FIG. 2. (a) The pulse sequences for the single-photon generation: (i) Doppler cooling for 6 μs. (ii) 300 ns-long pulse of the 397 nm laser to generate a single photon in the cavity. (iii) Recycling the ion's population back to the $S_{1/2}$ state for 500 ns. (iv) A pulse of the 866 nm laser is injected to the cavity. The 866 nm laser is frequency locked to the resonance to the $P_{1/2} - D_{3/2}$ transition. Therefore, its transmission peak provides an absolute frequency reference for Δ_c. (b) Single-photon emission spectrum as a function of Δ_c with Δ_p at -10 MHz. The solid line is a Lorentzian fit. The vertical dashed lines indicate the center frequency of the peak (black) and the frequency expected from the condition $\Delta_p = \Delta_c$ (red). The same applies to the dashed lines in (c). (c) Single-photon emission spectra with different Δ_p. From the top to the bottom traces, Δ_p varies from -20 to $+20$ MHz with an interval of 5 MHz. The traces are vertically offset to avoid overlapping. (d) The shift of the Raman resonance δ as a function of Δ_p from the data set in (c). The solid line is a fit by the numerical simulation. The inset figure shows superimposed traces of δ from numerical simulations with $g_0/(2\pi)$ varying from 13 to 16 MHz.

$$|u_0\rangle = \frac{g_2|a,1,0\rangle - g_1|b,0,1\rangle}{\lambda}, \tag{2}$$

where $\lambda = \sqrt{g_1^2 + g_2^2}$. Note that $|u_0\rangle$ is a dark state which is decoupled from the atomic upper state $|c\rangle$. The emergence of this state is very similar to the effect of electromagnetically induced transparency [38]. The difference here is that the quantized cavity fields, instead of classical lasers, interconnect the three atomic levels. On the other hand, a *bright state* can also be constructed as $|v\rangle = (g_1|a,1,0\rangle + g_2|b,0,1\rangle)/\lambda$ in which the excitation amplitudes to $|c,0,0\rangle$ from the constituent states interfere constructively. $|u_+\rangle$ and $|u_-\rangle$ can be expressed as

$$|u_\pm\rangle = \frac{|v\rangle \pm |c,0,0\rangle}{\sqrt{2}}, \tag{3}$$

with an energy gap of 2λ [Fig. 3(c)]. Consequently, in the same way as between $|g,1\rangle$ and $|e,0\rangle$ in the two-level case, the coherent oscillation occurs between $|v\rangle$ and $|c,0,0\rangle$ at a frequency of 2λ. This oscillation corresponds to the characteristic emission (and absorption) of a single photon into (and from) the two optical modes simultaneously in a superposition. Hence, the vacuum Rabi frequency—the frequency at which a single excitation is exchanged between the atomic and optical degrees of freedom—is given by $2g = 2\lambda$.

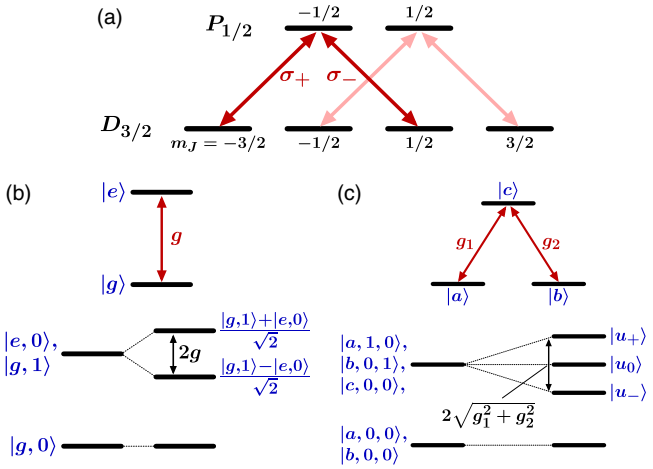

FIG. 3. (a) The Zeeman sublevels in the $P_{1/2}$ and $D_{3/2}$ state manifolds interacting with a bimodal cavity. (b) Top: A two-level atom coupled to a single optical mode with a coupling strength g. Bottom: The level diagram of the total energy of the system with (without) the atom-cavity coupling [right (left)]. (c) Top: A three-level atom coupled to two optical modes simultaneously with coupling strength g_1 and g_2, respectively. Bottom: The level diagram of the three-level bimodal system with (without) the atom-cavity coupling [right (left)]. The energy levels of the first excited states split into three levels with corresponding dressed states.

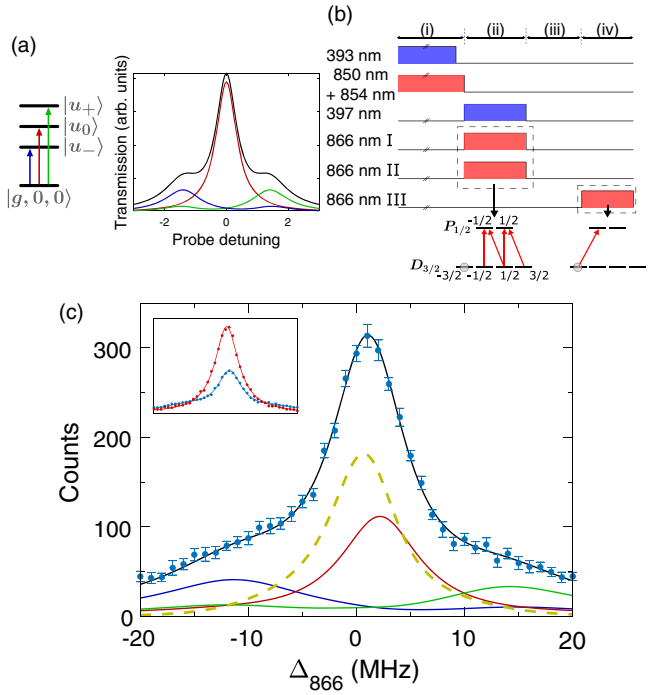

FIG. 4. (a) A model calculation for the ideal three-level system. The solid line shows the expected spectrum of transmitted photons as a function of the probe detuning. Here, $g_1 = g_2 = g$ and the probe frequency is normalized by g. The underlying contributions of the individual dressed states are shown in the same colors as the corresponding excitations in the level diagram on the left. (b) Laser pulse sequences: (i) 5 μs-long Doppler cooling. The duration of the repumping beams is longer than that of the 393 nm beam in order to prepare the ion in the $S_{1/2}$ state. (ii) Optical pumping for 3 μs. (iii) An interval to wait for the intensities of the optical pumping lasers to sufficiently diminish. (iv) Probing with beam III. (c) The counts of the transmitted photons of beam III as a function of its detuning. The background counts (~90) from stray light are subtracted. The solid black line is the result of numerical calculation (see the main text). The underlying contributions are also shown. In addition the contribution from nondressed states is shown in the yellow dashed line. The inset also shows a spectrum taken without the ion (red) superposed with the spectrum with the ion (blue).

Applying this picture to the actual energy levels of $^{40}Ca^+$ in Fig. 3(a), g_1 and g_2 are derived from g_0 by multiplication with the Clebsh-Gordan coefficients for the σ_+ and σ_- transitions, which are $1/\sqrt{2}$ and $1/\sqrt{6}$, respectively. With $g_0 = 2\pi \times (15.1 \pm 0.1)$ MHz, $g = 2\pi \times (12.3 \pm 0.1)$ MHz is obtained. Therefore, the coupling of the single ion to the cavity g exceeds both the atomic decay rate of the $P_{1/2}$ level γ ($=2\pi \times 11.5$ MHz) [36] and the cavity decay rate κ [$=2\pi \times (4.1 \pm 0.1)$ MHz], placing our system in the strong coupling regime ($g > \gamma, \kappa$).

The characteristic vacuum Rabi splitting in the three-level bimodal system as shown in Fig. 3(c) can be probed by weakly driving the cavity and detecting the transmission. Figure 4(a) shows the expected spectrum of the transmitted photons when the ideal three-level bimodal system is probed with a near-resonant coherent light. There are three underlying resonant peaks corresponding to the three distinct excitations from the ground state. Figure 4(b) shows the laser pulse sequences used to probe this in the experiment. Beams I and II of the 866 nm laser are applied with π and σ_- polarizations, respectively, in order to optically pump the ion into the $D_{3/2}$ $m_J = -3/2$ state. Subsequently, a pulse of beam III in the σ_+ polarization is injected and its transmission through the FFPC is measured. The FFPC is locked to the atomic resonance ($\Delta_c = 0$). The intensity of beam III in the cavity is estimated in terms of the displacement amplitude to the intracavity field [32]. Figure 4(c) shows the resulting spectrum of the transmitted photons as the detuning of beam III from the atomic resonance ($\equiv \Delta_{866}$) is scanned. The spectrum is significantly modified by the ion-cavity coupling [see the inset of Fig. 4(c)]. The data show good agreement with the numerical simulation shown as the black solid line in Fig. 4(c). Only the vertical scaling and a small horizontal offset (~0.47 MHz) are adjusted to fit the simulated curve to the measured data. The horizontal offset is likely to have resulted from an error in the calibration of the frequency of the 866 nm laser. The figure also shows the simulated contributions of the excitations to the individual dressed states and contribution from other states. There is a finite probability that the probing laser excites the ion and incoherently distributes its population via spontaneous decays from the $P_{1/2}$ state. This results in the transmission of subsequent photons without interacting with the ion and creates the central peak in a dashed yellow line in the figure. Note that this probability increases as g increases and hence progressively fewer photons are required to probe the system, whereas in practice a certain number of photons are required at the detector to ensure a decent signal-to-noise ratio. Despite this noise, the wings of the observed spectrum indicate the deviation from a single-peaked structure and the presence of the dressed states $|u_\pm\rangle$ with an expected separation of $2g$.

In conclusion, we have achieved the strong coupling regime for the first time with a single ion, where the vacuum Rabi frequency exceeds both atomic and cavity decoherence rates. Moreover, the characteristic energy structure of the dressed states inherent to our coupled ion-cavity system has been successfully probed by spectroscopic means. The key milestones that have led to this work are the overcoming of practical limitations that have limited the successful integration of an ion trap with a miniature cavity for decades and the ability to precisely control the ion's position in the cavity mode. Strong coupling between a single ion and an optical cavity facilitates novel opportunities to combine the unparalleled capabilities of trapped ions with quantum photonics. It enables applications such as highly efficient single-photon sources and high-fidelity ion-photon quantum interfaces, key components in quantum networks and

quantum computing. Without further optimization, a numerical study shows that a heralded entanglement efficiency of 1.7% at a rate of 8.5 kHz between two remote ions can be achieved, a factor of ∼1900 improvement over previous work [30]. Moreover, our FFPC can be readily modified to further enhance the single-photon generation efficiency by simply increasing the external coupling of one of the cavity mirrors or optimizing the mirror geometry [32,39].

We gratefully acknowledge support from EPSRC through EP/J003670/1 and the U.K. Quantum Technology Hub: NQIT-Networked Quantum Information Technologies (EP/M013243/1).

Note added in the proof.—Recently, we became aware of a work [40] that reports an enhanced entanglement generation rate between remotely trapped ions using fluorescence collection. Our cavity-based approach enables a further improvement by two orders of magnitude over the rate achieved in [40].

*takahashi@qiqb.otri.osaka-u.ac.jp

[1] H. J. Kimble, Phys. Scr. **T76**, 127 (1998).
[2] S. Girvin, M. Devoret, and R. Schoelkopf, Phys. Scr. **T137**, 014012 (2009).
[3] A. Boca, R. Miller, K. M. Birnbaum, A. D. Boozer, J. McKeever, and H. J. Kimble, Phys. Rev. Lett. **93**, 233603 (2004).
[4] P. Maunz, T. Puppe, I. Schuster, N. Syassen, P. W. H. Pinkse, and G. Rempe, Phys. Rev. Lett. **94**, 033002 (2005).
[5] J. P. Reithmaier, G. Sek, A. Löffler, C. Hofmann, S. Kuhn, S. Reitzenstein, L. V. Keldysh, V. D. Kulakovskii, T. L. Reinecke, and A. Forchel, Nature (London) **432**, 197 (2004).
[6] T. Yoshie, A. Scherer, J. Hendrickson, G. Khitrova, H. Gibbs, G. Rupper, C. Ell, O. Shchekin, and D. Deppe, Nature (London) **432**, 200 (2004).
[7] A. Wallraff, D. I. Schuster, A. Blais, L. Frunzio, J. Majer, S. Kumar, S. M. Girvin, and R. J. Schoelkopf, Nature (London) **431**, 162 (2004).
[8] I. Chiorescu, P. Bertet, K. Semba, Y. Nakamura, C. Harmans, and J. Mooij, Nature (London) **431**, 159 (2004).
[9] P. F. Herskind, A. Dantan, J. P. Marler, M. Albert, and M. Drewsen, Nat. Phys. **5**, 494 (2009).
[10] I. Shomroni, S. Rosenblum, Y. Lovsky, O. Bechler, G. Guendelman, and B. Dayan, Science **345**, 903 (2014).
[11] M. Scheucher, A. Hilico, E. Will, J. Volz, and A. Rauschenbeutel, Science **354**, 1577 (2016).
[12] G. R. Guthöhrlein, M. Keller, K. Hayasaka, W. Lange, and H. Walther, Nature (London) **414**, 49 (2001).
[13] A. B. Mundt, A. Kreuter, C. Becher, D. Leibfried, J. Eschner, F. Schmidt-Kaler, and R. Blatt, Phys. Rev. Lett. **89**, 103001 (2002).
[14] M. Keller, B. Lange, K. Hayasaka, W. Lange, and H. Walther, Nature (London) **431**, 1075 (2004).
[15] D. R. Leibrandt, J. Labaziewicz, V. Vuletić, and I. L. Chuang, Phys. Rev. Lett. **103**, 103001 (2009).
[16] J. D. Sterk, L. Luo, T. A. Manning, P. Maunz, and C. Monroe, Phys. Rev. A **85**, 062308 (2012).
[17] A. Stute, B. Casabone, P. Schindler, T. Monz, P. Schmidt, B. Brandstätter, T. Northup, and R. Blatt, Nature (London) **485**, 482 (2012).
[18] A. Stute, B. Casabone, B. Brandstätter, K. Friebe, T. Northup, and R. Blatt, Nat. Photonics **7**, 219 (2013).
[19] M. Steiner, H. M. Meyer, C. Deutsch, J. Reichel, and M. Köhl, Phys. Rev. Lett. **110**, 043003 (2013).
[20] T. G. Ballance, H. M. Meyer, P. Kobel, K. Ott, J. Reichel, and M. Köhl, Phys. Rev. A **95**, 033812 (2017).
[21] T. P. Harty, D. T. C. Allcock, C. J. Ballance, L. Guidoni, H. A. Janacek, N. M. Linke, D. N. Stacey, and D. M. Lucas, Phys. Rev. Lett. **113**, 220501 (2014).
[22] C. J. Ballance, T. P. Harty, N. M. Linke, M. A. Sepiol, and D. M. Lucas, Phys. Rev. Lett. **117**, 060504 (2016).
[23] C. W. Chou, D. B. Hume, J. C. J. Koelemeij, D. J. Wineland, and T. Rosenband, Phys. Rev. Lett. **104**, 070802 (2010).
[24] N. Huntemann, C. Sanner, B. Lipphardt, C. Tamm, and E. Peik, Phys. Rev. Lett. **116**, 063001 (2016).
[25] S. Kotler, N. Akerman, Y. Glickman, A. Keselman, and R. Ozeri, Nature (London) **473**, 61 (2011).
[26] I. Baumgart, J.-M. Cai, A. Retzker, M. B. Plenio, and C. Wunderlich, Phys. Rev. Lett. **116**, 240801 (2016).
[27] S. Debnath, N. M. Linke, C. Figgatt, K. A. Landsman, K. Wright, and C. Monroe, Nature (London) **536**, 63 (2016).
[28] T. Monz, D. Nigg, E. A. Martinez, M. F. Brandl, P. Schindler, R. Rines, S. X. Wang, I. L. Chuang, and R. Blatt, Science **351**, 1068 (2016).
[29] H. J. Kimble, Nature (London) **453**, 1023 (2008).
[30] D. Hucul, I. Inlek, G. Vittorini, C. Crocker, S. Debnath, S. Clark, and C. Monroe, Nat. Phys. **11**, 37 (2015).
[31] C. Crocker, M. Lichtman, K. Sosnova, A. Carter, S. Scarano, and C. Monroe, Opt. Express **27**, 28143 (2019).
[32] See Supplemental Material at http://link.aps.org/supplemental/10.1103/PhysRevLett.124.013602 for experimental details and numerical simulations.
[33] C. Monroe, R. Raussendorf, A. Ruthven, K. R. Brown, P. Maunz, L.-M. Duan, and J. Kim, Phys. Rev. A **89**, 022317 (2014).
[34] H. Takahashi, E. Kassa, C. Christoforou, and M. Keller, Phys. Rev. A **96**, 023824 (2017).
[35] E. Kassa, H. Takahashi, C. Christoforou, and M. Keller, J. Mod. Opt. **65**, 520 (2018).
[36] M. Hettrich, T. Ruster, H. Kaufmann, C. F. Roos, C. T. Schmiegelow, F. Schmidt-Kaler, and U. G. Poschinger, Phys. Rev. Lett. **115**, 143003 (2015).
[37] M. Albert, J. P. Marler, P. F. Herskind, A. Dantan, and M. Drewsen, Phys. Rev. A **85**, 023818 (2012).
[38] M. Fleischhauer, A. Imamoglu, and J. P. Marangos, Rev. Mod. Phys. **77**, 633 (2005).
[39] K. Ott, S. Garcia, R. Kohlhaas, K. Schüppert, P. Rosenbusch, R. Long, and J. Reichel, Opt. Express **24**, 9839 (2016).
[40] D. P. Nadlinger, B. C. Nichol, S. An, P. Drmota, T. G. Ballance, K. Thirumalai, J. F. Goodwin, D. M. Lucas, and C. J. Ballance, arXiv:1911.10841.